Published in final edited form as:
*Biochim Biophys Acta Biomembr*. 2018 March ; 1860(3): 664–672. doi:10.1016/j.bbamem.2017.12.001.

# Inhibition of mitochondrial UCP1 and UCP3 by purine nucleotides and phosphate

**Gabriel Macher**[1], **Melanie Koehler**[2,#], **Anne Rupprecht**[1], **Jürgen Kreiter**[1], **Peter Hinterdorfer**[2], and **Elena E. Pohl**[1,*]

[1]Institute of Physiology, Pathophysiology and Biophysics, University of Veterinary Medicine, Vienna, Austria

[2]Institute of Biophysics, Johannes Kepler University, Linz, Austria

## Abstract

Mitochondrial membrane uncoupling protein 3 (UCP3) is not only expressed in skeletal muscle and heart, but also in brown adipose tissue (BAT) alongside UCP1, which facilitates a proton leak to support non-shivering thermogenesis. In contrast to UCP1, the transport function and molecular mechanism of UCP3 regulation are poorly investigated, although it is generally agreed upon that UCP3, analogous to UCP1, transports protons, is activated by free fatty acids (FFA) and is inhibited by purine nucleotides (PN). Because the presence of two similar uncoupling proteins in BAT is surprising, we hypothesized that UCP1 and UCP3 are differently regulated, which may lead to differences in their functions. By combining atomic force microscopy and electrophysiological measurements of recombinant proteins reconstituted in planar bilayer membranes, we compared the level of protein activity with the bond lifetimes between UCPs and PNs. Our data revealed that, in contrast to UCP1, UCP3 can be fully inhibited by all PNs and IC50 increases with a decrease in PN-phosphorylation. Experiments with mutant proteins demonstrated that the conserved arginines in the PN-binding pocket are involved in the inhibition of UCP1 and UCP3 to different extents. Fatty acids compete with all PNs bound to UCP1, but only with ATP bound to UCP3. We identified phosphate as a novel inhibitor of UCP3 and UCP1, which acts independently of PNs. The differences in molecular mechanisms of the inhibition between the highly homologous transporters UCP1 and UCP3 indicate that UCP3 has adapted to fulfill a different role and possibly another transport function in BAT.

## Introduction

Proton transport across the inner mitochondrial membrane is essential for physiological processes such as heat production, as demonstrated for mitochondrial uncoupling protein 1,

*Author to whom correspondence should be addressed.
#Current address: Institute of Life Science, University Catholiqué de Louvain, Louvain-la-Neuve, Belgium

**Conflict of Interest**
The authors declare no conflict of interest.




Europe PMC Funders Author Manuscripts

UCP1 [1, 2], or the modulation of reactive oxygen species (ROS) production, as originally proposed for other members of the uncoupling protein family, including UCP3 [3, 4]. UCP3 is expressed in heart, skeletal muscles and, similar to UCP1, in brown adipose tissue [5, 6]. The presence of two uncoupling proteins in BAT is surprising and suggests that UCP1 and UCP3 may be differently regulated, which will enable them to fulfill different functions [6]. Thus far, studies using cell and animal models failed to show any clear phenotype or function of UCP3 [7–11]. Meanwhile evidence has emerged that UCP3 is highly abundant in cells and tissues with predominantly FA beta-oxidation type of metabolism [6, 8].

Although other transport functions, such as transport of free fatty acids [12, 13], were also proposed for UCP3, its ability to transport protons [14] remains unchallenged. The regulation of UCP3-mediated proton transport is mistakenly regarded as well-understood, in reference to the high homology of UCP3 to UCP1 (56 % for mice). There are several hypotheses which try to explain the mechanism of UCP1 activation by FA [15–19], but basically one mechanism was proposed for UCP1 inhibition by purine nucleotides (PNs) in the late ‘90s [20, 21]. According to this mechanism, three arginines (R83, R182 and R276), which are localized in the central cavity of UCP1, bind the phosphate groups of di- and tri-phosphate PNs, leading to a conformational change of protein and inhibition of proton transport. This regulatory mechanism has generally been extended to other UCPs, because these arginines are conserved in all UCP homologues. One of the few studies investigating this mechanism in UCP3 reported that, in contrast to UCP1, diphosphate- and not triphosphate- purine nucleotides are the strongest inhibitors of UCP3 [22]. In contrast, CD and fluorescence spectroscopy data revealed similar changes in UCP1 and UCP3 secondary structures upon binding of different PNs, whereby triphosphates exhibited the strongest effect [23].

The main goal of this work was to evaluate the molecular mechanism of UCP3’s inhibition in comparison to that of UCP1. For this, we performed a quantitative characterization of the UCP-PN interactions under various conditions using (i) electrophysiological measurements of the transmembrane current, (ii) high-resolution atomic force microscopy (AFM) and (iii) UCP1 and UCP3 mutants. A comparison of the structural information with functional data obtained for mutant and wild type proteins enabled us to update a model for the PN binding to UCP1 and to propose a novel mechanism for UCP3-PN binding.

## Materials and Methods

### Chemicals

*E.coli* polar lipid (EPL) was purchased from Avanti Polar Lipids (Alabaster, USA). 1,2-dioleoyl-sn-glycero-3-phosphocholine (DOPC), 1,2-dioleoyl-sn-glycero-3-phosphoethanolamine (DOPE), cardiolipin (CL from bovine heart), arachidonic acid (AA), Triton X-114 octylpolyoxyethylene, DTT, BSA, purine nucleotides, $Na_2SO_4$, $(NH_4)_2HPO_4$, MES, Tris, EGTA, hexane, hexadecane, SDS were obtained from Sigma-Aldrich (Munich, Germany). Chloroform was from Merck KGaA (Darmstadt, Germany) or from J.T. Baker (Griesheim, Germany), argon and nitrogen ($N_2$) - from Linde Gas GmbH (Stadl-Paura, Austria).

APTES obtained from Sigma Aldrich (Austria) was distilled at low pressure and stored under argon in sealed crimp vials over silica gel at -20 °C to avoid polymerization. TEA (Sigma Aldrich, Austria) was stored under argon and in the dark to avoid amine oxidation. The heterobifunctional crosslinker NHS-PEG-acetal was kindly provided by Hermann J. Gruber (Johannes Kepler University Linz, Austria) and used as described in [24]. The EDA derivates of the purine nucleotides, which were coupled to the AFM tip, 2′-/3′-O-(2-aminoethylcarbamoyl)-adenosine-5′- O-triphosphate (EDA-ATP), 2′-/3′-O-(2-aminoethylcarbamoyl)-adenosine-5′-O-diphosphate (EDA-ADP) and 2′-/3′-O-(2-aminoethylcarbamoyl)-adenosine-5′-O-monophosphate (EDA-AMP) were provided by BioLog (Bremen, Germany) in the form of sodium salt dissolved in a 10 mM aqueous solution.

All chemicals mentioned above were purchased in their highest available purity and stored as requested in the data sheet.

## Expression of mUCP1 and mUCP3, and their reconstitution into liposomes

Cloning and expression of mouse UCP1 (mUCP1) and mouse UCP3 (mUCP3) was carried out as described in [6, 25]. For protein reconstitution, 1 mg protein from inclusion bodies was solubilized in TE/G-buffer containing 2% SLS and 1 mM DTT and mixed gradually with 50 mg of EPL or 50 mg lipid mixture (LM: DOPC, DOPE and CL; 45:45:10 mol%) dissolved in TE/G-buffer with the addition of 1.3 % Triton X-114, 0.3% octylpolyoxyethylene, 1 mM DTT and GTP to a final concentration of 2 mM. After incubation overnight, the mixture was concentrated using Amicon Ultra-15 filters (Millipore, Schwalbach, Germany), dialyzed for 2 h against a TE/G-buffer with 1 mg/ml BSA and 1 mM DTT and then twice again overnight without DTT. Buffer exchange was carried out by three dialyses against an assay buffer (50 mM $Na_2SO_4$, 10 mM MES, 10 mM Tris, 0.6 mM EGTA at pH 7.35). Aggregated and unfolded proteins were eliminated by centrifugation of the dialysate at 14000 x g and application of a 0.5 g hydroxyapatite-containing column (Bio-Rad, Munich, Germany). Remaining detergent was removed by incubating twice with Bio-Beads SM-2 (Bio-Rad, Germany). The protein content of proteoliposomes was determined by Micro BCA Protein Assay (Perbio Science Deutschland GmbH, Bonn, Germany). The protein purity was verified by SDS-PAGE and silver staining. Proteoliposomes were stored at -80°C until used.

## Generation of UCP mutants

*In vitro* site-directed mutagenesis was carried out on expression plasmids containing the cDNA of mUCP1 [25] or mUCP3 [6] as templates. The mutations were introduced with designed oligonucleotides to alter the following codons: mUCP1 Arg84 (AGG) to Gln (CAG), mUCP1 Arg183 (AGA) to Thr (ACA), mUCP1 Arg277 (CGA) to Leu (CTA), mUCP3 Arg84 (CGC) to Gln (CAG), mUCP3 Arg184 (AGA) to Thr (ACA) and mUCP3 Arg278 (CGT) to Leu (CTT) using a QuikChange II site-directed mutagenesis kit (Agilent, Austria). Successful mutations of the expression plasmids were confirmed by sequencing. Mutant UCP expression plasmids were transformed in the *E. coli* expression strain Rosetta. Expression induction, inclusion body isolation and reconstitution into liposomes of UCP mutants were performed as described above for UCP wildtypes.

### Formation of planar bilayer membranes and measurement of membrane electrical parameters

Planar lipid bilayers were formed from (proteo)liposomes as described previously [26]. If not mentioned otherwise, all experiments were carried out using a lipid concentration of 1.5 mg/ml at 32°C. Fatty acids were added directly to the membrane-forming lipid solution in a concentration of 10 or 15 mol%.

Membrane formation was monitored by measuring the specific membrane capacitance, which was typically 0.73 ± 0.5 μF/cm$^2$ and did not depend on protein, AA and PN content. Current-voltage (I/V) characteristics were measured by a patch-clamp amplifier (EPC 10, HEKA Elektronik, Dr. Schulze GmbH, Germany). The total membrane conductance (G) at zero voltage was calculated from a linear fit of experimental current (I) data [25]. We assume that protein molecules were randomly (approx. 50:50%) oriented in free standing bilayer membranes used for electrophysiology and in supported bilayers used for AFM measurements (s. below). In electrophysiological experiments we applied voltage from -50 mV to +50 mV allowing us to measure currents through protein oriented to both sides.

To compare different charges of recombinant proteins (s. below and Fig. S1, A), we calculated relative conductance according to Equation 1,

$$G_{rel} = \frac{G - G_0}{G_1 - G_0} \quad (1)$$

where $G_0$ is the total membrane conductance of lipid membranes reconstituted with AA, $G_1$ is the total membrane conductance of lipid membranes reconstituted with UCPs and AA, and G is the total membrane conductance of lipid membranes reconstituted with UCPs, AA and inhibitors (Fig. 1, A). The membrane proton conductance was measured and the protein turnover number for mUCP3 was calculated as described in [18].

Curve fitting was performed in SigmaPlot using a four parameter logistic regression fit (2),

$$y = d + \frac{a - d}{1 + (\frac{x}{c})^b} \quad (2)$$

Where ***y*** is the relative conductance, ***x*** the inhibitor concentration, the maximum asymptote ***d*** is the remaining relative conductance at maximum inhibition, the inflection point ***c*** is the IC50, ***a*** is the relative conductance without inhibitors and ***b*** is Hill's slope of the curve.

In this study, we compared the activity of UCP1 in model membranes made from E.coli polar lipid (EPL) and a mixture of DOPC, DOPE and cardiolipin (LM). Previously, we determined by GC–MS analysis ([27], Suppl. Fig. 9) that EPL contains approx. 36% 16:0, 8% 16:1, 32% 18:1, 10% cyclo FA and small amounts of 12:0, 14:0 and 18:0 fatty acids. In contrast, the LM we used contains approx. 79% 18:1, 19% 18:2 and small amounts of 16:0, 18:0, 20:3 and 20:4 (for exact. data see [27]) and is more physiological. Fig. S1, A shows

that UCP1 reconstituted in LM in the presence of arachidonic acid exhibited higher membrane conductance in comparison to that reconstituted in EPL. The comparison of relative conductance (ratio between G after activation to G after inhibition) demonstrated, however, that regulation of UCP activity does not depend on the lipid composition (Fig. S1, B).

### Tip chemistry for binding studies using AFM

Commercial silicon-nitride AFM cantilevers (MSNL levers, Bruker) were functionalized with the ethylene diamine derivate of either ATP, ADP or AMP (EDA-ATP, 2′ -/3′-O-(2-aminoethylcarbamoyl)-adenosine-5′-O-triphosphate, -diphosphate, -monophosphate, Biolog) as described before for ATP [24].

### AFM measurements and data analysis

All measurements were performed using a PicoPlus 5500 AFM (Keysight Technologies Inc.). Freshly cleaved mica (Christine Groepl, Electron Microscopy, Tulln, Austria) was placed in the center of the AFM sample plate and mounted with a flow-through fluid cell. UCP-containing proteoliposomes were pipetted into the fluid cell on the mica surface and incubated for 10 min. For PN-FA competition experiments, UCP-containing proteoliposomes were mixed with AA-containing liposomes in required proportions to a final lipid concentration of 1 mg/(ml of assay buffer). For the formation of supported membranes we used E. coli polar lipid (EPL). Fig. S1, B demonstrates that the relative conductance of membranes made from different lipids (EPL or lipid mixture DOPC/DOPE/CL (LM)) was similar.

Since UCP can only be reconstituted in the supported lipid membrane at low lateral density, a combination of recognition imaging and force spectroscopy for mapping and studying the interaction between mUCP1 and PNs was applied as described in [28]. Proteins that showed strong binding in the TREC mode were selected for further detailed analysis using force spectroscopy.

The lifetime of PN-UCP interactions was calculated using a maximum likelihood fitting routine and the Bell-Evans Model (Table S1). In this approach, every single unbinding event with their respective loading rate (and therefore spring constant) is plotted against the measured unbinding force on a semi-logarithmic scale and fitted by utilizing the maximum likelihood fitting routine [29].

### Statistical analysis

Data are presented as mean values of at least three independent experiments ± SD or SE, as noted in the figure description.

## Results

### 1 The mUCP3 proton transfer rate is comparable with those of mUCP1 and mUCP2

To test whether mUCP3 reconstituted in planar lipid membranes can be activated by free fatty acids (FA) and inhibited by purine nucleotides (PN) similar to hamster UCP1 and

human UCP2 [18, 30], we measured current-voltage (I/V) characteristics in the presence of (i) arachidonic acid (AA), or (ii) mUCP3 and AA, or (iii) mUCP3, AA and ATP. Fig. 1, A shows that I and G are increased in the presence of mUCP3 and AA, and decreased after addition of 2 mM ATP, as demonstrated previously for UCP1 (Fig. S1, A [18]) and UCP2 [30]. The addition of α-cyclodextrin demonstrates a decrease of membrane total conductance due to extraction of FA from the membrane (Fig. S2), supporting the necessity of fatty acids for the activation of UCP3.

To assess the proton transport rate of mUCP3, $\kappa$, we measured the contribution of the proton conductance, $G_{H/OH}$, to the total G. Fig. 1, B shows that a formation of the pH gradient across a membrane reconstituted with AA and mUCP3 led to a shift in the reversal potential of the I/V characteristics that was used to calculate $\kappa$. The value $\kappa$=2.56 ±0.79 $s^{-1}$, obtained from seven independent experiments, was comparable to $\kappa$ previously estimated for UCP1 and UCP2 [18, 30].

## 2 Inhibition of mUCP3 by purine nucleotides (PN) exhibits different features compared to mUCP1

Next, we measured whether the inhibition of mUCP3 depends on PN phosphorylation and PN concentration. Fig. 2, A shows that ATP is the strongest inhibitor that achieves maximum inhibition at a concentration of approx. 4 mM, followed by ADP and AMP. We confirmed previous reports that ATP similarly inhibits mUCP1 and mUCP3 in proteoliposomes [31]. However, we revealed that whereas all PN were able to fully inhibit mUCP3 at high PN concentrations, ADP and AMP were only able to partially inhibit mUCP1. Maximum inhibition (Fig. 2, C) and IC50 values (Fig. 2, D, Table S1) were calculated by fitting of the mUCP3 (Fig. 2, A) and mUCP1 (Fig. 2, B) inhibition data (see Materials and Methods). IC50 estimated for mUCP3 increased with a decrease in the level of PN-phosphorylation in contrast to mUCP1, which exhibited the same IC50 for all three PNs.

## 3 Binding of purine nucleotides to mUCP3 correlates with the degree of PN-mediated inhibition

To elucidate whether PN-UCP bond lifetime determines PN inhibitory potency, we applied a combination of topographical, recognition (TREC) and force modes of AFM [28]. Attachment of PN to the cantilever enabled the identification and quantification of protein–nucleotide interactions simultaneously to target protein imaging and provided information about UCP-topography and UCP-PN binding (Fig. 3, A, inset). Fig. 3, A shows a representative loading rate dependence plot for the determination of the mUCP3-ATP binding force. Interestingly, the lifetime of both mUCP3-PN (1.33 s, 0.56 s and 0.13 s for ATP, ADP and AMP respectively) and mUCP1-PN (1.12 s, 0.75 s and 0.16 s for ATP, ADP and AMP respectively) interactions decreases alongside with the degree of PN-phosphorylation (Fig. 3, B). The results correspond to the overall strength of PN inhibition that also decreases with PN-phosphorylation (Fig. 2, A and B).

$x_\beta$ values (Fig. S3, Table S4) were similar for all PNs and both proteins. This parameter can be correlated with the binding length [32], indicating that all PNs are positioned very similarly inside the UCPs and that phosphates always bind the same residues.

## 4 Binding of free fatty acids affects UCP-PN inhibition and shows differences between mUCP1 and mUCP3

Competition between FFAs and GDP has been shown for UCP1, but still has not yet been reported for UCP3 or for any other PNs in the case of UCP1. Inhibition (relative conductance, Fig. 4, A and Table S2) and binding (life time, Fig. 4, B and Table S2) of ATP, ADP and AMP were measured at different arachidonic acid (AA) concentrations (10 and 15 mol%). The inhibitory effect of ATP on mUCP3 was higher at lower AA concentration, while the inhibition by other PNs showed less (ADP) or no (AMP) dependence on AA concentration. In contrast, mUCP1 inhibition by all PNs correlated with the AA concentration (Fig. 4, A). The maximum inhibition of mUCP1 by ADP or AMP is lower than 100% in the presence of 15 mol% AA (Fig. 2, C). We therefore tested, whether it is also increased in the presence of lower FFA concentrations (Fig. S4). mUCP1 inhibition was dependent on FFA concentration, but only at lower ADP concentrations. No change in maximum inhibition was apparent, but IC50 was affected by FFA concentration. These results imply that mUCP3 and mUCP1 show a different dependence on PN-phosphorylation due to the PN-FFA competition. To understand whether this behavior is reflected in PN-UCP binding, we measured lifetimes with the same loading rates as mentioned above in the presence of either 10 mol% or 15 mol% AA (Fig. 4, B, Table S2). In the presence of 15 mol % AA, the lifetimes were significantly increased for both UCP1 and UCP3 interactions with ATP and the UCP1-ADP interaction. The increase of the UCP3-ADP lifetime in the presence of 15 mol % AA was not significant and the interactions of both proteins with AMP were unaffected by the AA concentration.

## 5 Mutations of key arginine residues indicates crucial differences between UCP1 and UCP3 in the molecular mechanisms of PN-inhibition

Because the molecular mechanism proposed for the UCP1-GDP interaction [20, 21] was unable to sufficiently describe the observed behavior of UCP1 and since no mechanism has yet been proposed for UCP3, we decided to re-evaluate the role of the three key arginine residues which were hypothesized to interact with PNs in mUCP1 (R277, R183 and R84) for all PNs and to evaluate the respective residues in mUCP3 (R278, R184 and R84). The replaced amino acids were chosen to eliminate the positive charge of arginine (see Materials and Methods). We further performed experiments to evaluate the inhibition of mUCP1- and mUCP3-mutants by ATP, ADP and AMP. Fig. 5, A reveals that the mutation of R278 led to no differences in inhibition between mutated and wild type (wt) forms of mUCP3. We, however, observed a very strong change in mUCP3 inhibition in the R184T mutation. All PNs, independent of their phosphorylation, were unable to inhibit the proton leak by any degree. mUCP3R84Q decreased the strength of ATP and ADP inhibition but did not affect AMP-mediated inhibition.

Fig. 5, B demonstrates that the respective mutants of mUCP1 showed distinctively different effects compared to their mUCP3 counterparts. Inhibition by ATP was similarly reduced in all three mUCP1 mutants and was comparable to the inhibition degree of mUCP1 wt in the presence of ADP. While mutation of R84Q did not affect the inhibition of mUCP1 in the presence of ADP and AMP respectively, the mUCP1R183T mutant showed an impaired inhibition by ADP but not AMP. Interestingly, the introduction of R277L mutation led to an

overall decrease of mUCP1 inhibition in parallel with the phosphorylation state of PN. The inhibition of mUCP1R277L in the presence of ATP or ADP was similar to that of mUCP1 wt, in the presence of ADP and AMP respectively. AMP was no longer able to inhibit mUCP1R277L.

### 6 Inorganic phosphate, $P_i$, inhibits UCP1 and UCP3 by a different mechanism compared to PNs

In addition to the fact that the inhibition of UCPs by PNs depends on binding of the phosphate groups, we now demonstrated that a single phosphate-UCP3 interaction led to full inhibition of protein activity. Because a substantial pool of inorganic phosphate ($P_i$) is present in mitochondria alongside with PNs, we tested whether $P_i$ also affects the UCP1 and UCP3 activity. Fig. 6, A shows that the inhibition degree of mUCP3 (green) and mUCP1 (blue) increases with a boost in $P_i$ concentration. For mUCP3, unlike inhibition with PNs, only partial inhibition could be achieved at the maximal $P_i$ concentration. Curve fitting of the inhibition data of mUCP3 allows calculation of the maximum inhibition (~60%) and IC50 values (~1 mM) (Fig. 6, B, Table S3), which were similar to mUCP1. Interestingly, none of the arginine mutations had any effect on the inhibition of mUCP3 by phosphate (Fig. 6, C). This shows that phosphate inhibition utilizes a completely different mechanism than inhibition by PNs.

## Discussion

In this study we have demonstrated that recombinant mUCP3 reconstituted in free-standing bilayer membranes conducts protons in the presence of unsaturated arachidonic acid. The idea that UCP3 may be involved in BAT thermogenesis, compensating for insufficient uncoupling by UCP1, has recently gained attention again. It has been shown that UCP1/UCP3 double knockout mice are even more cold-sensitive than $UCP1^{-/-}$ mice [33]. In this study we revealed that the UCP3 proton transfer rate is roughly the same as that of UCP1 and UCP2 [18, 30]. In combination with its lower expression, which is even lower if UCP1 is knocked out [6], we assume that UCP3 cannot compensate for thermogenesis if UCP1 is impaired.

The UCP3-PN bond lifetimes, $\tau$, determined from directly measured dissociation forces, have shown that $\tau$ decreases with a decreasing number of PN phosphate groups, which correlates with the inhibitory capacity of PN. Previously, only association/dissociation constants were measured either in the presence of detergents [34], which may affect protein secondary structure and folding [35] or by using dansylated-PNs, where the fluorescent group may have exerted a drastic effect on PN inhibition [34].

Our results confirmed that three arginine residues, R277, R183 and R84, are involved in the interaction of UCP1 with PNs as previously proposed [20]. We have also demonstrated (Fig. 7, A) that these residues bind the $\gamma-$, $\beta-$ and $\alpha-$phosphates of PNs. Since ADP inhibition was unaffected by the R84Q mutation in mUCP1, we cannot confirm that the $\beta$-phosphate of ADP binds to both R84 and R183 of mUCP1. We propose that each arginine-phosphate (R-P) interaction makes a contribution to the same extent, resulting in complete inhibition only in the case where three phosphate moieties are bound. This contradicts the earlier model that

proposes that inhibition solely depends on the R277- α-phosphate interaction and that binding to all three residues is essential for inhibition. The partial maximum inhibition of ADP and AMP (Fig. 2, B) and the fact that mutants retain some inhibition capacity, if not all P-R interactions are affected (Fig. 5, B), support our point of view. In contrast to previous postulates that monophosphates are unable to bind to mUCP1 and that di- and triphosphates bind to identical residues in UCP1, we have now demonstrated the binding of AMP and inhibition by AMP, as well as significant differences between ATP and ADP binding. Previous studies, especially during the late 1990s and early 2000s, utilized very low concentrations of PNs in combination with low membrane potentials, created by ion gradients in liposomes. Since UCP inhibition is non-linearly dependent on membrane potential [25], this could explain why others have failed to detect inhibition by AMP.

Based on the results of the present study, we propose the first mechanism of UCP3 inhibition by PNs (Fig. 7, B). According to this mechanism, the interaction of R184 in UCP3 with the α-phosphate of PNs is essential for the inhibition of proton transport and by itself causes full inhibition. Binding of the β- and γ-phosphates to additional residues inside the UCP3 PN-binding-pocket further strengthens the PN-UCP3 interaction which causes a decrease in the IC50. R84 interacts with the β-phosphate while UCP3 amino acid residue(s) that bind the γ-phosphate remained unknown. We assume that a mutation of this unknown residue exhibits effects similar to that of mUCP3R84Q, but that it only affects inhibition by ATP. R277 is not a part of the UCP3-PN binding-pocket. Our results clearly showed that inhibition of UCP3 as well as PN-UCP3 bond lifetime increases with an increase in PN-phosphorylation and that triphosphate-PNs are the most potent inhibitors and binding partners. It is similar to the UCP1 inhibition mechanism, but contradicts earlier reports that mono-phosphate cannot inhibit UCP3 and that diphosphate-PNs are the most potent inhibitors of UCP3 [22, 31]. Our data are supported by the observation which is based on the changes in UCP3 helical content by CD [23], that triphosphate-PN had the strongest effect on UCP3 and showed that, although AMP exhibits the weakest binding to UCP3 and the lowest IC50 among the tested PNs, it can fully inhibit UCP3.

We, for the first time, describe a direct competition between FFAs and PNs during activation/inhibition of UCP3. This type of competition is controversially discussed for UCP1 [15, 19, 36]. For UCP2, Berardi and Chou [37] advanced the hypothesis that conformational changes after binding of either PNs or FFAs cause the displacement of the other compound. This hypothesis could explain our experimental results for UCP1, where the effect of all PNs is affected by FFA concentration. However, it failed to explain the competition of only triphosphates with FFAs in UCP3. We therefore propose for UCP3 that this competition primarily depends on interactions between the PN γ-phosphate and the FFAs. PN-UCP bond lifetime (Fig. 4, B) decreases with a decrease in FFA concentration, which could be associated with less inhibition. The observed effect is strongest for ATP, much weaker for ADP (no longer significant in case of UCP3) and absent for AMP. In previous studies the displacement of PNs by FFAs was shown after application of transmembrane potential [19], while the displacement of FFAs by PNs was shown in the absence of potential [37]. It's a possibility, that we did not see the displacement of the tip-bound PN from UCP in the presence of AA, because transmembrane potential would be required but could not be applied in AFM experiments. Furthermore, the free movement of

PNs may be decreased due to their attachment to the AFM tip via a chemical linker. It was reported that FFA-binding loosens up the helix packing of UCPs [38]. This could allow tip bound PNs to bind easier, resulting in stronger binding and increased τ in the presence of more AA.

Strikingly, we identified inorganic phosphate ($P_i$) as a new inhibitor of UCPs. Inhibition by $P_i$ does not show the differences between UCP1 and UCP3, which we described for PN-mediated inhibition. Phosphate causes similar partial inhibition of UCP1 and UCP3, where mutations have no effect on the inhibition (Fig. 6, C). We therefore propose that $P_i$ acts through a unique and independent mechanism compared to PNs. Previously we have shown that PNs can bind UCPs from both the matrix and the cytosolic side but only cause inhibition when bound from the cytosol [24]. $P_i$, however, is even significantly smaller than AMP, allowing for greater maneuverability and accessibility in the central cavity of UCPs. Therefore, it is difficult to say whether $P_i$ inhibition has a similar preference for either the matrix or the cytosolic side. Since the physiological phosphate concentrations in the intermembrane space is ~3 mM and even higher (>10 mM), in the mitochondrial matrix [39], $P_i$ inhibition, with an IC50 of 1mM, is of great physiological importance in both cases.

In summary, the molecular mechanisms of the inhibition depict significant differences in the regulation of highly homologous proteins UCP1 and UCP3, and indicate that UCP3 has adapted to fulfill a different role and possibly another transport function in BAT.

## Supplementary Material

Refer to Web version on PubMed Central for supplementary material.

## Acknowledgements

We are grateful to Sarah Bardakji for help with recombinant protein preparation and Olga Jovanovic for valuable discussion. We thank Quentina Beatty for editorial assistance as a native English speaker. This work was supported by Austrian Research Fund (FWF, P 25357-B20 to EEP).

## Abbreviations

| | |
|---|---|
| **AA** | arachidonic acid |
| **AFM** | atomic force microscopy |
| **BAT** | brown adipose tissue |
| **BSA** | albumin from bovine serum |
| **CL** | cardiolipin from bovine heart |
| **DOPC** | 1,2-dioleoyl-sn-glycero-3-phosphocholine |
| **(α-CD)** | alpha-cyclodextrin |
| **DOPE** | 1,2-dioleoyl-sn-glycero-3-phosphoethanolamine |
| **DTT** | dithiothreitol |

Europe PMC Funders Author Manuscripts

| | |
|---|---|
| **EGTA** | ethylene glycol-bis(β-aminoethyl ether)-N,N,N',N'-tetraacetic acid |
| **EPL** | E.coli polar lipid extract |
| **FFA** | free fatty acid |
| **IMM** | inner mitochondrial membrane |
| **MES** | 2-(N-morpholino) ethanesulfonic acid |
| **PN** | purine nucleotide |
| **ROS** | reactive oxygen species |
| **TREC** | simultaneous topography and recognition imaging by AFM |
| **Tris** | tris(hydroxymethyl)amino-methane |
| **UCP** | uncoupling proteins |

## References


1. Nicholls DG, Locke RM. Thermogenic mechanisms in brown fat. Physiol Rev. 1984; 64:1–64. [PubMed: 6320232]
2. Cannon B, Nedergaard J. Brown adipose tissue: function and physiological significance. Physiol Rev. 2004; 84:277–359. [PubMed: 14715917]
3. Krauss S, Zhang CY, Lowell BB. The mitochondrial uncoupling-protein homologues. Nat Rev Mol Cell Biol. 2005; 6:248–261. [PubMed: 15738989]
4. Skulachev VP. Uncoupling: new approaches to an old problem of bioenergetics. Biochim Biophys Acta. 1998; 1363:100–124. [PubMed: 9507078]
5. Boss O, Samec S, Paoloni-Giacobino A, Rossier C, Dulloo A, Seydoux J, Muzzin P, Giacobino JP. Uncoupling protein-3: a new member of the mitochondrial carrier family with tissue-specific expression. FEBS Lett. 1997; 408:39–42. [PubMed: 9180264]
6. Hilse KE, Kalinovich AV, Rupprecht A, Smorodchenko A, Zeitz U, Staniek K, Erben RG, Pohl EE. The expression of UCP3 directly correlates to UCP1 abundance in brown adipose tissue. Biochim Biophys Acta. 2016; 1857:72–78. [PubMed: 26518386]
7. Vidal-Puig AJ, Grujic D, Zhang CY, Hagen T, Boss O, Ido Y, Szczepanik A, Wade J, Mootha V, Cortright R, Muoio DM, et al. Energy metabolism in uncoupling protein 3 gene knockout mice. J Biol Chem. 2000; 275:16258–16266. [PubMed: 10748196]
8. Aguer C, Piccolo BD, Fiehn O, Adams SH, Harper ME. A novel amino acid and metabolomics signature in mice overexpressing muscle uncoupling protein 3. FASEB J. 2017; 31:814–827. [PubMed: 27871066]
9. Nowinski SM, Solmonson A, Rundhaug JE, Rho O, Cho J, Lago CU, Riley CL, Lee S, Kohno S, Dao CK, Nikawa T, et al. Mitochondrial uncoupling links lipid catabolism to Akt inhibition and resistance to tumorigenesis. Nat Commun. 2015; 6:8137. [PubMed: 26310111]
10. Nabben M, van Bree BW, Lenaers E, Hoeks J, Hesselink MK, Schaart G, Gijbels MJ, Glatz JF, da Silva GJ, De Windt LJ, Tian R, et al. Lack of UCP3 does not affect skeletal muscle mitochondrial function under lipid-challenged conditions, but leads to sudden cardiac death. Basic Res Cardiol. 2014; 109:447. [PubMed: 25344084]
11. Zhang CY, Hagen T, Mootha VK, Slieker LJ, Lowell BB. Assessment of uncoupling activity of uncoupling protein 3 using a yeast heterologous expression system. FEBS Lett. 1999; 449:129–134. [PubMed: 10338118]
12. Aguer C, Fiehn O, Seifert EL, Bezaire V, Meissen JK, Daniels A, Scott K, Renaud JM, Padilla M, Bickel DR, Dysart M, et al. Muscle uncoupling protein 3 overexpression mimics endurance

training and reduces circulating biomarkers of incomplete beta-oxidation. FASEB J. 2013; 27:4213–4225. [PubMed: 23825224]

13. Schrauwen P, Hesselink MK. The role of uncoupling protein 3 in fatty acid metabolism: protection against lipotoxicity? Proc Nutr Soc. 2004; 63:287–292. [PubMed: 15294045]
14. Zackova M, Jezek P. Reconstitution of novel mitochondrial uncoupling proteins UCP2 and UCP3. Biosci Rep. 2002; 22:33–46. [PubMed: 12418549]
15. Winkler E, Klingenberg M. Effect of fatty acids on H+ transport activity of the reconstituted uncoupling protein. J Biol Chem. 1994; 269:2508–2515. [PubMed: 8300577]
16. Jezek P, Modriansky M, Garlid KD. A structure-activity study of fatty acid interaction with mitochondrial uncoupling protein. FEBS Lett. 1997; 408:166–170. [PubMed: 9187360]
17. Skulachev VP. Fatty acid circuit as a physiological mechanism of uncoupling of oxidative phosphorylation. FEBS Lett. 1991; 294:158–162. [PubMed: 1756853]
18. Urbankova E, Voltchenko A, Pohl P, Jezek P, Pohl EE. Transport kinetics of uncoupling proteins:Analysis of UCP1 reconstituted in planar lipid bilayers. J Biol Chem. 2003; 278:32497–32500. [PubMed: 12826670]
19. Fedorenko A, Lishko PV, Kirichok Y. Mechanism of fatty-acid-dependent UCP1 uncoupling in brown fat mitochondria. Cell. 2012; 151:400–413. [PubMed: 23063128]
20. Modriansky M, Murdza ID, Patel HV, Freeman KB, Garlid KD. Identification by site-directed mutagenesis of three arginines in uncoupling protein that are essential for nucleotide binding and inhibition. J Biol Chem. 1997; 272:24759–24762. [PubMed: 9312070]
21. Klingenberg M. Wanderings in bioenergetics and biomembranes. Biochim Biophys Acta. 2010; 1797:579–594. [PubMed: 20175988]
22. Zackova M, Skobisova E, Urbankova E, Jezek P. Activating omega-6 polyunsaturated fatty acids and inhibitory purine nucleotides are high affinity ligands for novel mitochondrial uncoupling proteins UCP2 and UCP3. J Biol Chem. 2003; 278:20761–20769. [PubMed: 12670931]
23. Ivanova MV, Hoang T, McSorley FR, Krnac G, Smith MD, Jelokhani-Niaraki M. A comparative study on conformation and ligand binding of the neuronal uncoupling proteins. Biochemistry. 2010; 49:512–521. [PubMed: 20000716]
24. Zhu R, Rupprecht A, Ebner A, Haselgrubler T, Gruber HJ, Hinterdorfer P, Pohl EE. Mapping the nucleotide binding site of uncoupling protein 1 using atomic force microscopy. J Am Chem Soc. 2013; 135:3640–3646. [PubMed: 23414455]
25. Rupprecht A, Sokolenko EA, Beck V, Ninnemann O, Jaburek M, Trimbuch T, Klishin SS, Jezek P, Skulachev VP, Pohl EE. Role of the transmembrane potential in the membrane proton leak. Biophys J. 2010; 98:1503–1511. [PubMed: 20409469]
26. Beck V, Jaburek M, Breen EP, Porter RK, Jezek P, Pohl EE. A new automated technique for the reconstitution of hydrophobic proteins into planar bilayer membranes. Studies of human recombinant uncoupling protein 1. Biochim Biophys Acta. 2006; 1757:474–479. [PubMed: 16626624]
27. Jovanovic O, Pashkovskaya AA, Annibal A, Vazdar M, Burchardt N, Sansone A, Gille L, Fedorova M, Ferreri C, Pohl EE. The molecular mechanism behind reactive aldehyde action on transmembrane translocations of proton and potassium ions. Free Radic Biol Med. 2015; 89:1067–1076. [PubMed: 26520807]
28. Koehler M, Gabriel M, Rupprecht Anne, Zhu Rong, Gruber Hermann J, Pohl Elena E, Hinterdorfer Peter. Combined Recognition Imaging and Force Spectroscopy: A New Mode for Mapping and Studying Interaction Sites at Low Lateral Density. Science of Advance Materials. 2017; 9:7.
29. Wildling L, Unterauer B, Zhu R, Rupprecht A, Haselgrubler T, Rankl C, Ebner A, Vater D, Pollheimer P, Pohl EE, Hinterdorfer P, et al. Linking of Sensor Molecules with Amino Groups to Amino-Functionalized AFM Tips. Bioconjug Chem. 2011; 22:1239–1248. [PubMed: 21542606]
30. Beck V, Jaburek M, Demina T, Rupprecht A, Porter RK, Jezek P, Pohl EE. Polyunsaturated fatty acids activate human uncoupling proteins 1 and 2 in planar lipid bilayers. FASEB J. 2007; 21:1137–1144. [PubMed: 17242157]
31. Jaburek M, Garlid KD. Reconstitution of recombinant uncoupling proteins: UCP1, -2, and -3 have similar affinities for ATP and are unaffected by coenzyme Q10. J Biol Chem. 2003; 278:25825–25831. [PubMed: 12734183]

32. Baumgartner W, Hinterdorfer P, Schindler H. Data analysis of interaction forces measured with the atomic force microscope. Ultramicroscopy. 2000; 82:85–95. [PubMed: 10741656]
33. Riley CL, Dao C, Kenaston MA, Muto L, Kohno S, Nowinski SM, Solmonson AD, Pfeiffer M, Sack MN, Lu Z, Fiermonte G, et al. The complementary and divergent roles of uncoupling proteins 1 and 3 in thermoregulation. J Physiol. 2016
34. Huang SG, Lin QS, Klingenberg M. Slow-phase kinetics of nucleotide binding to the uncoupling protein from brown adipose tissue mitochondria. J Biol Chem. 1998; 273:859–864. [PubMed: 9422742]
35. Hoang T, Smith MD, Jelokhani-Niaraki M. Expression, folding, and proton transport activity of human uncoupling protein-1 (UCP1) in lipid membranes: evidence for associated functional forms. J Biol Chem. 2013; 288:36244–36258. [PubMed: 24196960]
36. Shabalina IG, Jacobsson A, Cannon B, Nedergaard J. Native UCP1 displays simple competitive kinetics between the regulators purine nucleotides and fatty acids. J Biol Chem. 2004; 279:38236–38248. [PubMed: 15208325]
37. Berardi MJ, Chou JJ. Fatty acid flippase activity of UCP2 is essential for its proton transport in mitochondria. Cell Metab. 2014; 20:541–552. [PubMed: 25127353]
38. Hoang T, Matovic T, Parker J, Smith MD, Jelokhani-Niaraki M. Role of positively charged residues of the second transmembrane domain in the ion transport activity and conformation of human uncoupling protein-2. Biochemistry. 2015; 54:2303–2313. [PubMed: 25789405]
39. Akerboom TPM, Bookelman H, Zuurendonk PF, van der Meer R, Tager JM. Intramitochondrial and Extramitochondrial Concentrations of Adenine Nucleotides and Inorganic Phosphate in Isolated Hepatocytes from Fasted Rats. European Journal of Biochemistry. 1978; 84:413–420. [PubMed: 639797]


Europe PMC Funders Author Manuscripts

Europe PMC Funders Author Manuscripts

## Highlights

- UCP3 has a unique PN-binding mechanism, different from UCP1.
- UCP-PN bond lifetimes correlate with PN-phosphorylation and inhibitory strength.
- Inorganic phosphate is a new physiologically relevant inhibitor of UCP1 and UCP3.

Europe PMC Funders Author Manuscripts

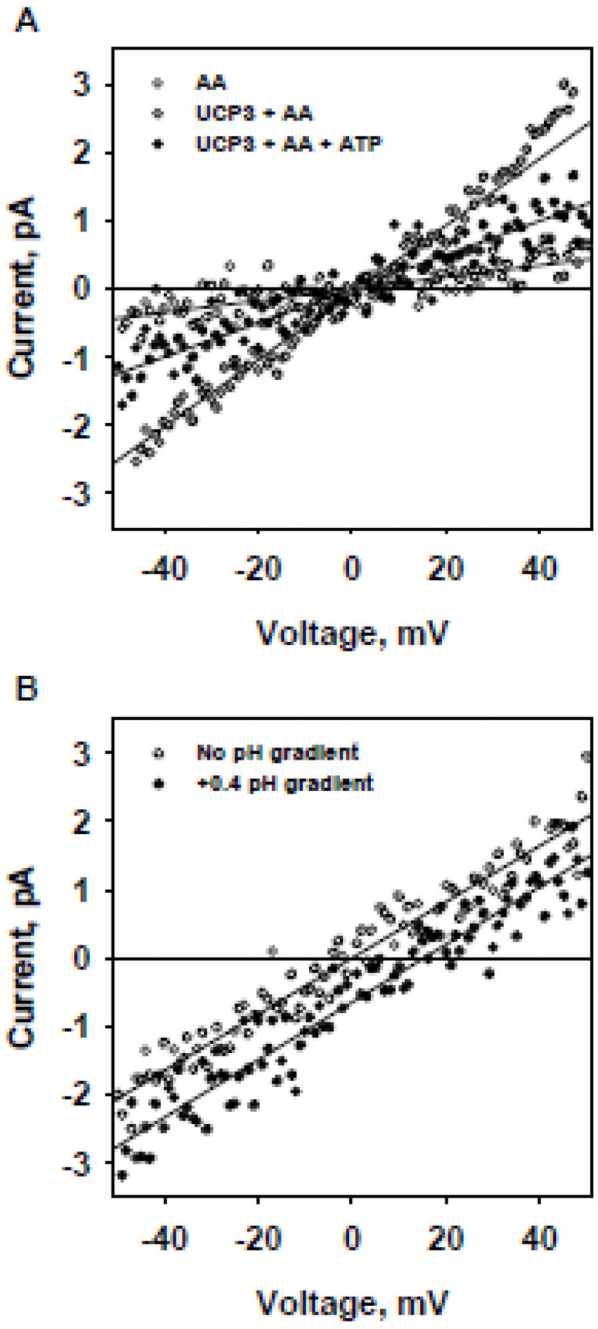


**Figure 1.**

**A.** Representative current-voltage (I/V) characteristics of membranes reconstituted with (i) arachidonic acid (AA, white), with AA and mUCP3 (grey), and in the presence of AA, mUCP3 and 2 mM ATP (black). The slope of I/V curves correlates with the total membrane conductance, G, and represents protein activity. **B.** Representative current-voltage characteristics of membranes reconstituted with mUCP3 and AA in the absence (white) and presence (black) of a transmembrane pH gradient. The induced shift of the reversal potential (= transmembrane current at 0 mV) was used to determine the proton transfer rate. Bilayer

membranes were made of 1.5mg/ml DOPC/DOPE/CL (45/45/10 mol%) reconstituted with 15 mol% AA. Protein concentration was 6 μg/(mg lipid) (UCP3, Charge 24). Buffer solution contained 50 mM $Na_2SO_4$, 10 mM MES, 10 mM Tris, 0.6 mM EGTA at pH 7.35 and T = 32°C.



Europe PMC Funders Author Manuscripts

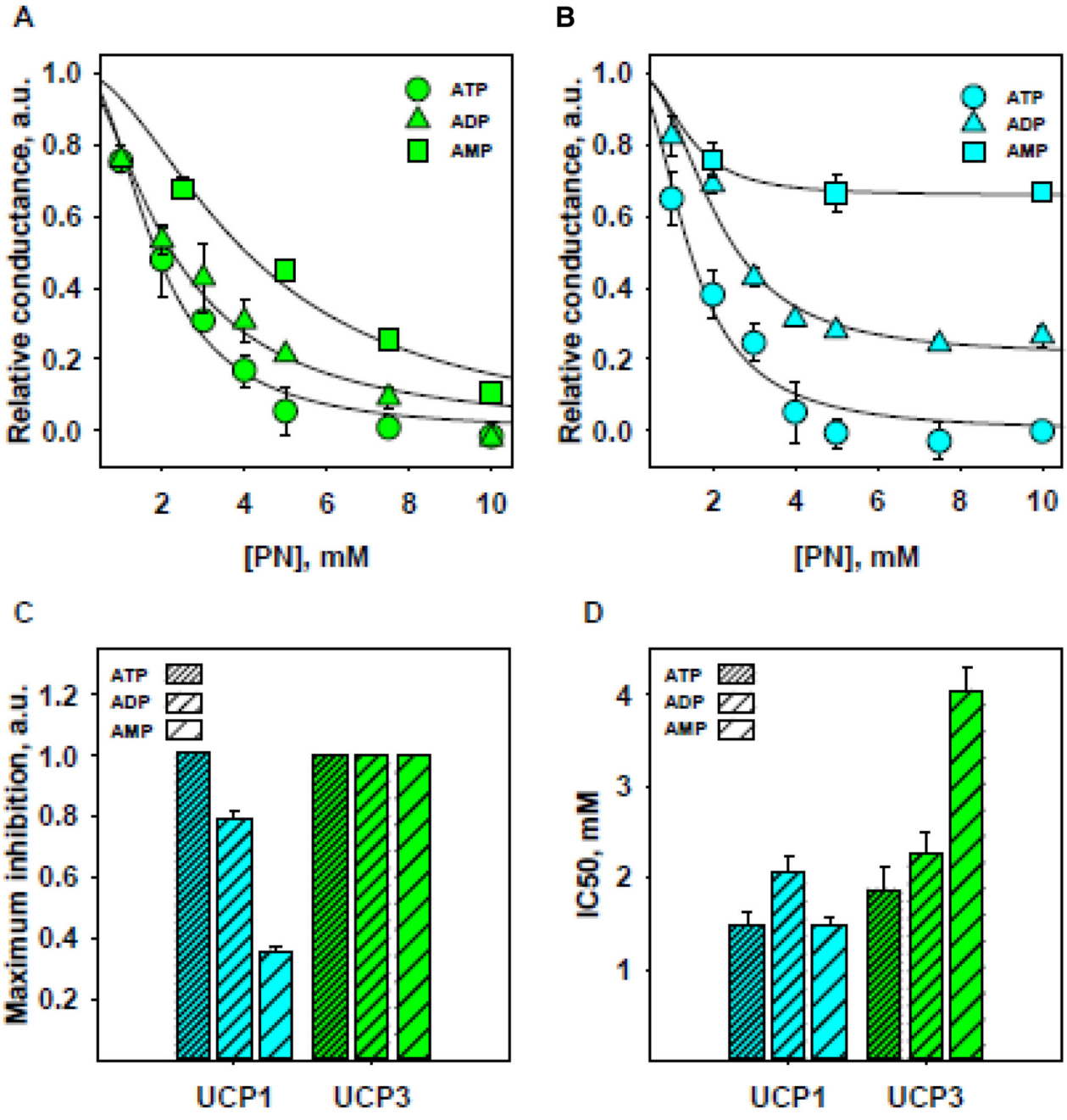


**Figure 2. Dependence of UCP3 proton transfer activity inhibition on purine nucleotide concentration and phosphorylation.**

**A, B.** Dependence of the relative conductance of UCP3 (green) or UCP1 (blue) on PN concentration in the presence of either ATP (circles), or ADP (triangles) or AMP (squares). Relative conductance describes the ratio between the total membrane conductance in the presence and absence of PN, with reference to the minimal possible membrane conductance (see Materials and Methods). Bilayer membranes made of DOPC/DOPE/CL (45/45/10) were reconstituted with 15 mol% AA. Buffer solution contained 50 mM $Na_2SO_4$, 10 mM

MES, 10 mM Tris, 0.6 mM EGTA at pH 7.35 and T = 32°C. Data represents mean values ± SD of at least 3 independent experiments. **C** and **D.** Maximum inhibition and IC50 of UCP3 inhibition (green) by PNs in comparison to UCP1 (blue), depending on PN-phosphorylation. Data shows mean values ± SD determined by fitting of data in Fig. 2, A and B (see Materials and Methods).



Europe PMC Funders Author Manuscripts

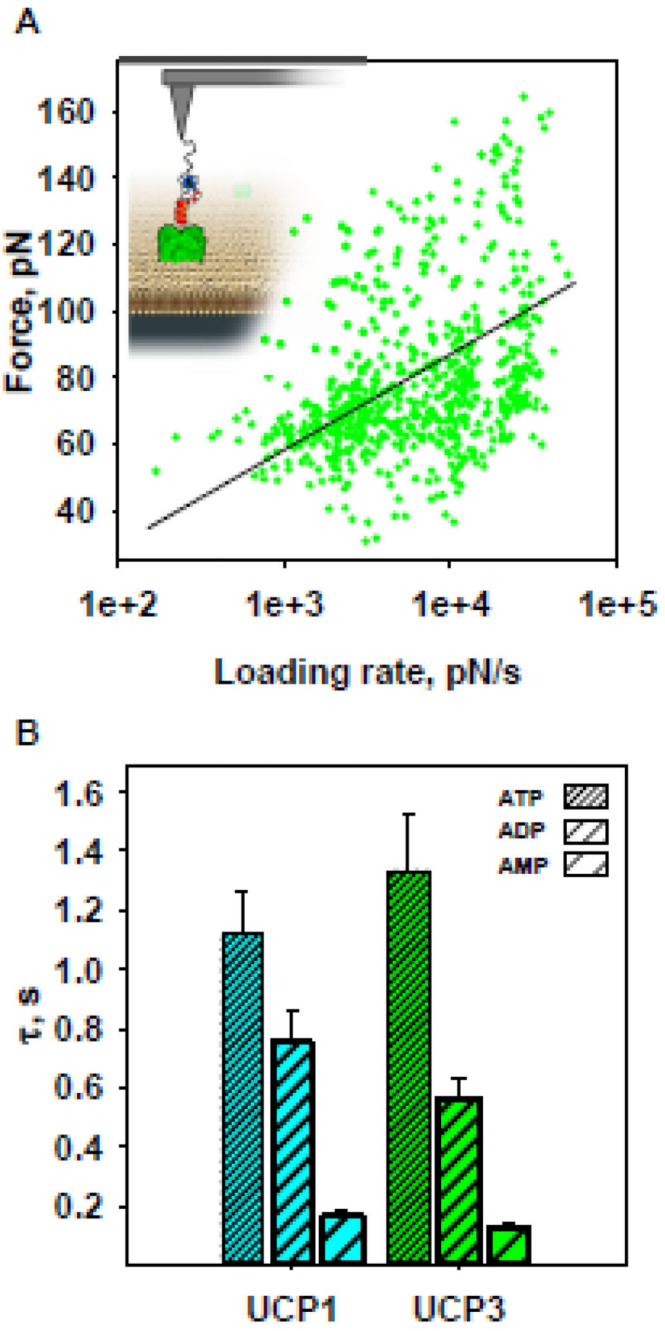


**Figure 3. Binding characteristics of UCP3-PN and UCP1-PN interactions.**

**A.** Schematic depiction of AFM measurements (inset) and representative loading rate dependence of UCP3-ATP unbinding forces, from which the bond lifetimes were directly determined. Rupture forces of all measured binding events between tip-bound ATP and protein are plotted against the effective spring constant of the cantilever, multiplied with the pulling speed (loading rate). Figure shows 932 binding events measured on a single UCP3. **B.** Dependence of lifetimes (τ) on PN-phosphorylation for UCP1-PN (blue) and UCP3-PN (green). Supported bilayer membranes were made of *E. coli* polar lipid extract, reconstituted

with UCP1/UCP3. Buffer solution contained 50 mM $Na_2SO_4$, 10 mM MES, 10 mM Tris, 0.6 mM EGTA at pH 7.35 and T = 21°C. Data represent mean values ± SD of at least three independent experiments.



Europe PMC Funders Author Manuscripts

Europe PMC Funders Author Manuscripts

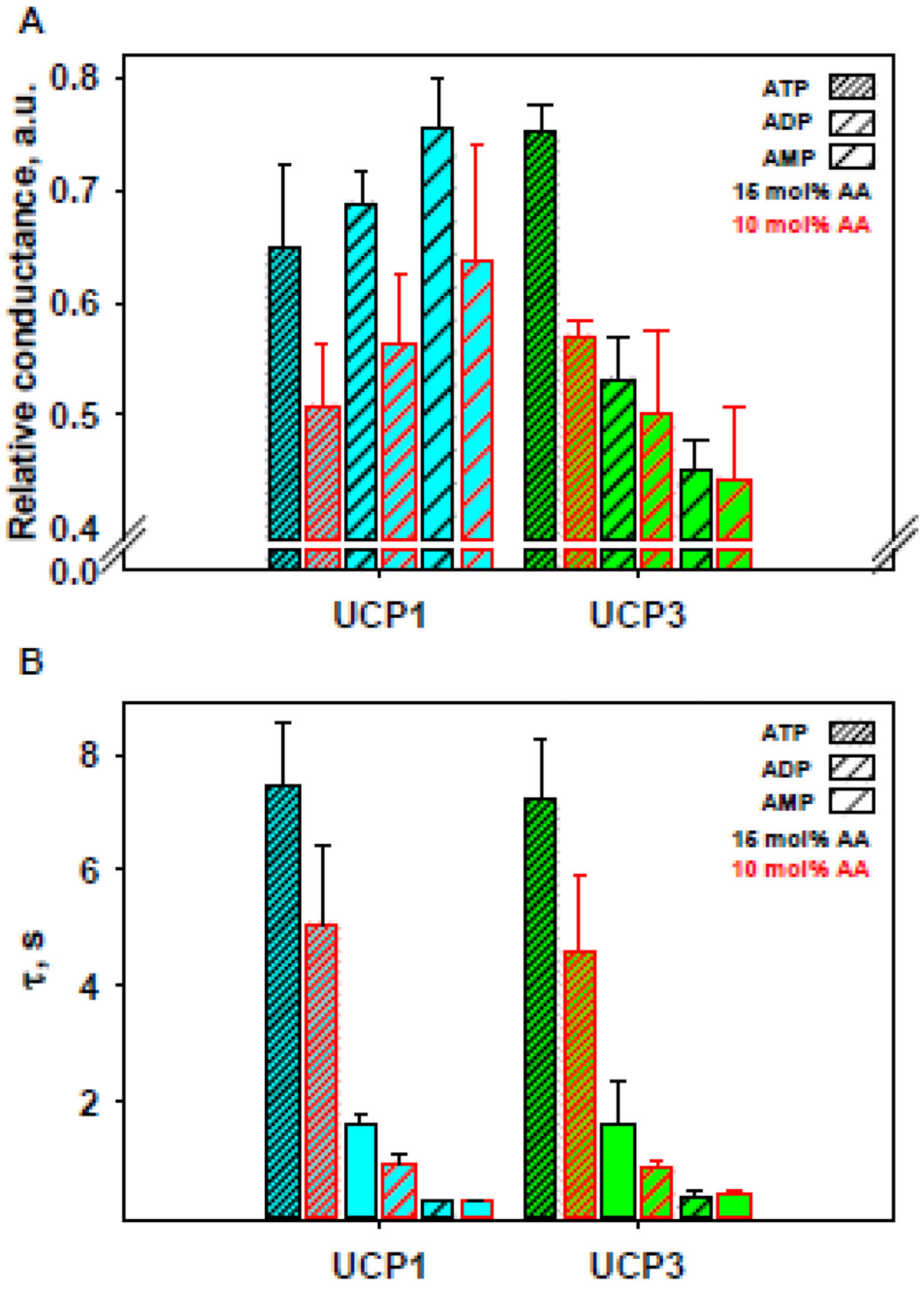


**Figure 4. Effect of free fatty acid concentration on UCP-PN binding and inhibition.**

**A.** Inhibition of UCP1 (blue) and UCP3 (green) by ATP (fine stripes), ADP (medium stripes) and AMP (coarse stripes) in the presence of either 15 mol% AA (black lines) or 10 mol% AA (red lines). PN concentrations were 1 mM ATP or 2 mM ADP for both proteins or 2 mM AMP for UCP1 and 5 mM AMP for UCP3. Bilayer membranes were made of DOPC/DOPE/CL (45/45/10). Buffer solution contained 50 mM $Na_2SO_4$, 10 mM MES, 10 mM Tris, 0.6 mM EGTA at pH 7.35 and T = 32°C. Data represents mean values ± SD of at least three independent experiments. **B.** Dependence of lifetimes (τ) on PN-phosphorylation for

UCP1-PN (blue) and UCP3-PN (green) in the presence of different concentration of AA. Bilayer membranes were made of EPL. Buffer solution contained 50 mM $Na_2SO_4$, 10 mM MES, 10 mM Tris, 0.6 mM EGTA at pH 7.35 and T = 21°C. Data represents mean values ± SD of at least three independent experiments.



Europe PMC Funders Author Manuscripts

Europe PMC Funders Author Manuscripts

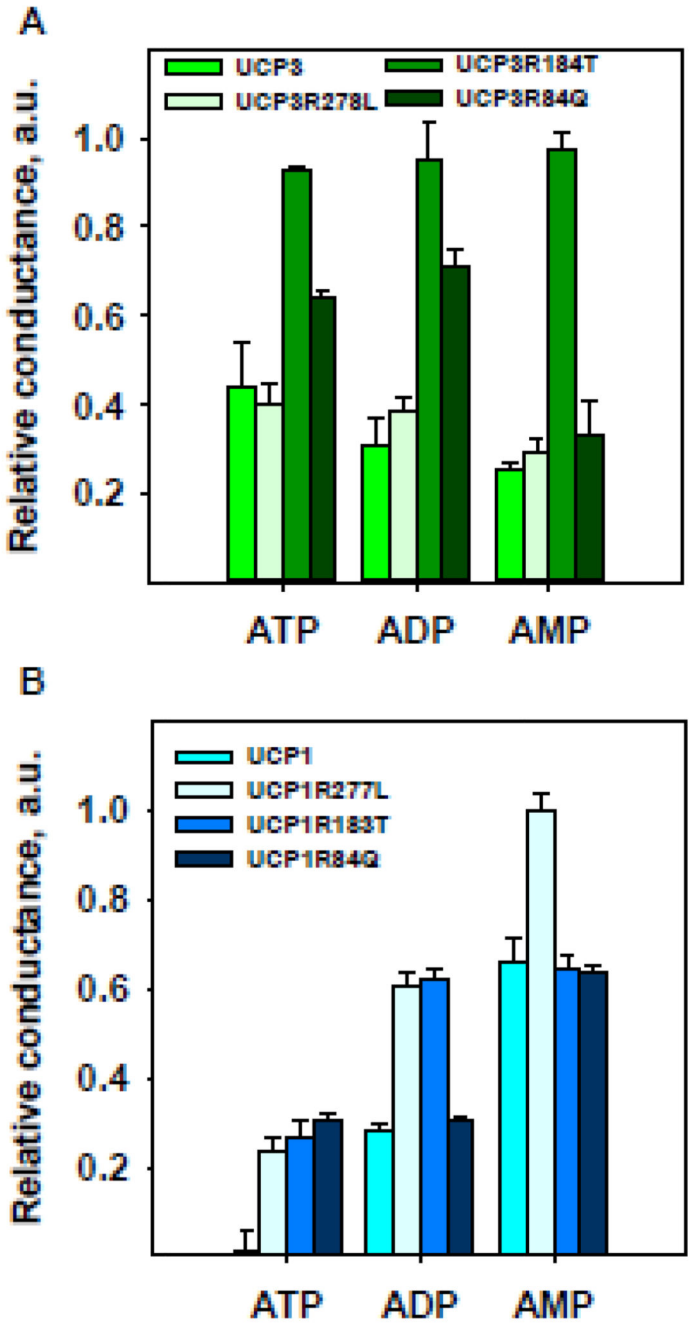


**Figure 5. Effect of point mutations on PN-mediated UCP1 and UCP3 inhibition.**

**A.** Relative conductance of UCP3 mutants (R278L, R184T and R84Q) in comparison to UCP3wt after inhibition with either 2 mM ATP, or 4 mM ADP, or 8 mM AMP. **B.** Relative conductance of UCP1 mutants (R277L, R183T and R84Q) in comparison to UCP1 wt after inhibition with either ATP, or ADP, or AMP. PN concentration was 5 mM. Bilayer membranes were made of DOPC/DOPE/CL (45/45/10) reconstituted with 15 mol% AA. Buffer solution contained 50 mM $Na_2SO_4$, 10 mM MES, 10 mM Tris, 0.6 mM EGTA at pH 7.35 and T = 32°C. Data represents means ± SD of at least three independent experiments.

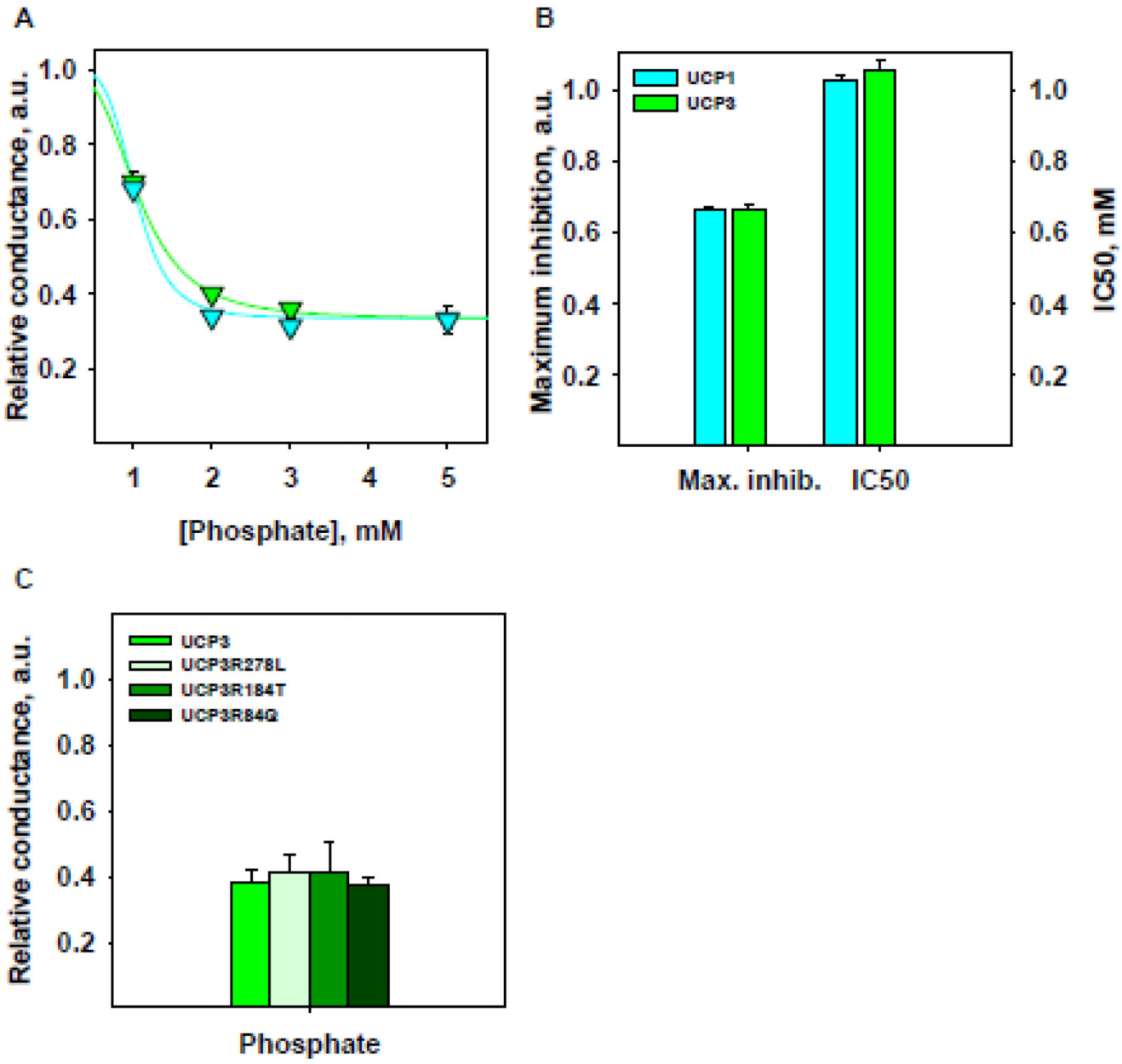


**Figure 6. Inhibition of UCP3 by inorganic phosphate, $P_i$.**

**A.** Dependence of relative conductance of UCP1 (blue) and UCP3 (green) on phosphate concentration. Bilayer membranes were made of DOPC/DOPE/CL (45/45/10) reconstituted with 15 mol% AA. Buffer solution contained 50 mM $Na_2SO_4$, 10 mM MES, 10 mM Tris, 0.6 mM EGTA at pH 7.35 and T = 32°C. Data represents mean values ± SD of at least three independent experiments.

**B.** Maximum inhibition and IC50 of UCP3 (green) and UCP1 (blue) in the presence of phosphate. Data shows mean values ± SD determined by fitting of data from Fig. 6, A (see Materials and Methods).

**C.** Relative conductance of UCP3 mutants (R278L, R184T and R84Q) in comparison to UCP3wt after inhibition with 3 mM ammonium-phosphate-dibasic. Bilayer membranes were made of DOPC/DOPE/CL (45/45/10) reconstituted with 15 mol% AA. Buffer solution contained 50 mM $Na_2SO_4$, 10 mM MES, 10 mM Tris, 0.6 mM EGTA at pH 7.35 and T = 32°C. Data represents means ± SD of at least three independent experiments.



Europe PMC Funders Author Manuscripts

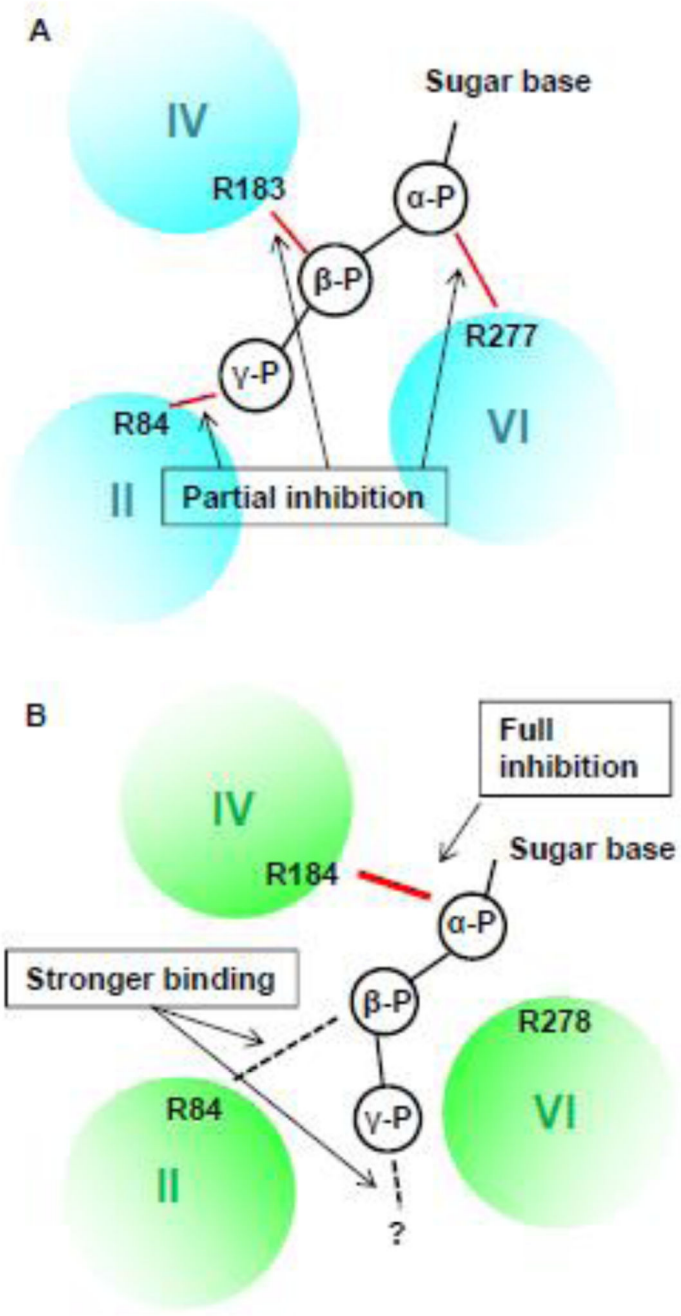


**Figure 7. Mechanisms of UCP-PN interaction and inhibition.**

**A.** Updated mechanism of UCP1 inhibition by PNs. We confirmed binding of R277, R183 and R84 to the α-, β- and γ- phosphate of PNs, respectively. There is no interaction between R84 and the β-phosphate of diphosphate-PNs. Each of these three P-R interactions independently and additively contributes to the maximum inhibition, but none of these interactions are essential for inhibition or PN-binding.

**B.** Novel mechanism of UCP3 inhibition by PNs. R184 interacts with the PN α-phosphate and is essential for protein inhibition. We propose that this interaction causes the

conformational change that leads to the inhibition in UCP3. R84 interacts with the β-phosphate and increases the binding strength, decreasing IC50. R278 is not a part of the UCP3 PN-binding-pocket. We further propose that another residue is part of the UCP3 PN-binding-pocket which acts like R84, but only interacts with the γ-phosphate.



Europe PMC Funders Author Manuscripts